

Time–Energy Quantum Uncertainty: Quantifying the Effectiveness of Surface Defect Passivation Protocols for Low-Dimensional Semiconductors

Nasir Alfaraj,^{*,†} Wael Alghamdi,[†] Meshal Alawein, Idris A. Ajia, Davide Priante, Bilal Janjua, Haiding Sun, Tien Khee Ng, Boon S. Ooi, Iman S. Roqan, and Xiaohang Li^{*}



Cite This: *ACS Appl. Electron. Mater.* 2020, 2, 409–418



Read Online

ACCESS |



Metrics & More

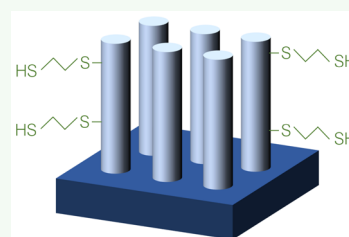


Article Recommendations



Supporting Information

ABSTRACT: The degree of enhancement in radiative recombination in ensembles of semiconductor nanowires after chemical treatment is quantified within a derived limit by correlating the energy released during the photoemission processes of the light–matter reaction and the effective carrier recombination lifetimes. It is argued that the usage of surface recombination velocity or surface saturation current density as passivation metrics that assess the effectiveness of surface passivation does not provide *strict* and *universal* theoretical bounds within which the degree of passivation can be *confined*. In this context, the model developed in this study provides a broadly applicable surface passivation metric for direct energy bandgap semiconductor materials. This is because of its reliance on the dispersion in energy and lifetime of electron–hole recombination emission at room temperature, in lieu of the mere dependence on the ratio of peak emission spectral intensities or temperature- and power-dependent photoluminescence measurements performed prior and subsequent to surface treatment. We show that the proposed quantification method, on the basis of steady-state and transient photoluminescence measurements performed entirely at room temperature, provides information about the effectiveness of surface state passivation through a comparison of the dispersion in carrier lifetimes and photon energy emissions in the nanowire ensemble before and after surface passivation. Our measure of the effectiveness of a surface passivation protocol is in essence the supremum of lower bounds one can derive on the product of Δt and ΔE .



$$0 \leq \frac{\Delta_\gamma}{\Delta_\varepsilon} \leq 1$$

KEYWORDS: defects, nanowires, photoluminescence, radiative recombination, surface states, time–energy dispersion, uncertainty

1. INTRODUCTION

Owing to the higher surface-area-to-volume ratios in lower-dimensional semiconductor structures and the subsequent induction of forbidden energy-band transitions caused by surface trap states,^{1–3} the intrinsic properties of d -dimensional semiconductor structures for all $d \in \{0, 1, 2\}$ are directly influenced by their surface condition.^{4–8} To help mitigate this issue, researchers have used sulfides (such as thiol-bond containing chemicals) for the surface passivation of group III–nitride nanostructured materials, via forming strong covalent/dative bonds between material surface and sulfur atoms.^{9,10} Zhao et al. investigated the passivation of InGaN/GaN multiple quantum disc (MQDisc) nanowire-based light-emitting diode (LED) devices by 1-octadecanethiol (ODT, $\text{CH}_3(\text{CH}_2)_{17}\text{SH}$) to modify the surface charge dynamics by weakening the band bending, thereby recovering the band-edge emission.¹¹ However, 1-octadecanethiol passivation has the potential of negatively influencing the operational stability and optoelectronic performance of nanowire-based devices. Khan et al. examined the spatiotemporal dynamics (generated by the Lie algebra relations $[r_k, r_n] = 0$ and $[r_k, t] = i\lambda_p r_k$ on the commutators¹² for the spatial variables r_j and the time variable

t , where λ_p is the Planck time) in as-grown and passivated InGaN nanowires and reported that 1-octadecanethiol passivation of the nanowires renders them covered by an amorphous polymeric coating. The coating was a result of severe polymeric deposition because of the long carbon chain in 1-octadecanethiol. Comparatively, 1,2-ethanedithiol (EDT, $\text{HSCH}_2\text{CH}_2\text{SH}$), having a much shorter carbon chain, can mitigate the polymeric deposition and thus preserve the integrity of the nanowires.^{9,13} Whereas 1-octadecanethiol and 1,2-ethanedithiol are organic chemical compounds, potassium hydroxide (KOH) is an elementary and nontoxic inorganic compound that was previously used to suppress surface recombination in AlGaIn nanowires¹⁴ and is commonly used in semiconductor chip fabrication.^{15,16} Yet, the aforementioned reports lack discussions of physical insights into the extent of the *goodness* of nanowire surface passivation through quantum

Received: September 6, 2019

Accepted: January 5, 2020

Published: January 5, 2020



mechanical descriptions and criteria that set theoretical bounds. Such theoretical bounds provide a fundamental scale of descriptions that define relevant and universal figures of merit to assess the effectiveness of passivation protocols. This is accomplished by scaling the effectiveness of passivation protocols in an inequality where dispersion in lifetime and energy are confined via a Heisenberg uncertainty relation. Further restriction of such a relation should correlate with worse passivation, a situation in which a passivation did not accomplish a remarkable change in the optoelectronic properties of the photoexcited nanowire ensemble. In particular, when a passivation process does not alter the optoelectronic properties of the nanowires, the product of the dispersions in lifetime and energy is no longer only known to be greater than Heisenberg's lower limit $\hbar/2$; rather, it should be close to the original product before implementing the passivation process.

Figure 1 illustrates common electronic absorption energy-band transitions in a direct energy bandgap semiconductor. In a wide bandgap semiconductor with high density of impurities

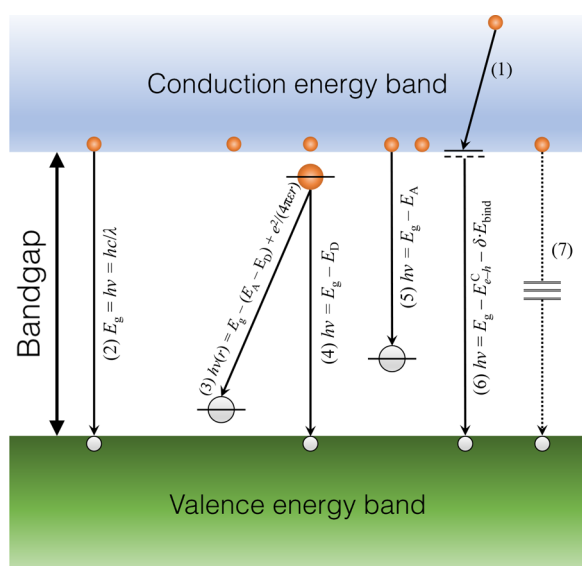


Figure 1. Simplified schematic illustration of exciton recombination paths in direct bandgap semiconductors: (1) intraband transition, whereby hot electrons relax their energy primarily by emitting phonons can also emit photons (this process is rare, as it involves many particles such as hot electrons under the assistance of either other electrons and phonons^{24–26}); (2) band-to-band transition; (3) shallow donor-to-shallow acceptor transition, where e is the elementary charge and r is the orbital radius of an excited state; (4) donor-to-valence-band transition; (5) conduction-band-to-acceptor transition; (6) free and bound excitonic transitions; and (7) surface states reaction sites, with energy eigenvalues given by $E = [V^2 - (q\hbar^2/ma)^2]^{1/2} \pm \hbar^2/2m[(\pi/a)^2 - q^2]$, where V is the surface potential, m is the charge carrier mass, \hbar is the Dirac constant, $k = \pm\pi/a$ is the Brillouin zone boundary, and q is a quantization parameter (for all energy levels of the surface states to be within the band gap, we must have $q \in [0, \pi m a V \hbar^2]$).^{27,28} Other transitions not shown here include donor-to-conduction band and acceptor-to-valence band. E_g is the energy bandgap, h is Planck's constant, c is the speed of light, E_{e-h}^C is the Coulombic interaction energy between the electron and electron hole, δE_{bind} is the exciton–donor/acceptor binding energy ($\delta = 0$ for free excitons whereas $\delta = 1$ for excitons bound to donors/acceptors), and E_D and E_A are the donor and acceptor levels, respectively.

and defects, photoluminescence (PL) can originate from deep- and shallow-level defect states, hence showing photoluminescence signatures centered at photon emission energies below its energy bandgap value (transitions (3), (4), and (5)).^{17,18} Moreover, surface defect states are continuum states and may cause band bending in the energy band structure of the nanowires. In general, band bending causes photoemission from the conduction band at different energy levels compared to that of flat energy bands. In our case, such band bending causes band-to-band photon emission having lower energy.¹ This happens at the surface, but in the bulk of nanowire structures, we should observe flat energy band emission. In fact, GaN-based nanowires generally suffer from oxygen and nitrogen vacancies ($V_{\text{O,N}}$) that act as surface defect states.¹⁹ As a consequence, surface passivation would improve the photoemission characteristics and reduce its peak width.^{20–22} It is worth noting that when nanowire surfaces are passivated, no additional radiative centers are introduced because the density of states (DOS) in the valence and conduction band edges remain unchanged ($D_{\text{1D}}(E)$); while nanowire surfaces are two-dimensional (2D)²³. Rather, the intensity of photoemission is affected. Therefore, rather than basing our assessment of passivation effectiveness merely on the ratio of peak photoluminescence emission intensities prior and subsequent to surface state passivation, as currently demonstrated in various literature, the present work utilizes the dispersion in spectral emission lines. By incorporating the dispersion in emission lines into our model, we thereby are aligning it more with the physical reality that band bending occurs and causes lower energy emission as observed in prior photoluminescence studies.

In this article, we execute a quantitative study of the surface passivation effects on 1,2-ethanedithiol-treated $\text{In}_{0.32}\text{Ga}_{0.68}\text{N}/\text{GaN}$ and potassium hydroxide-treated $\text{Al}_{0.14}\text{Ga}_{0.86}\text{N}/\text{Al}_{0.30}\text{Ga}_{0.70}\text{N}$ nanowires using steady-state and transient photoluminescence. We previously studied the photoinduced entropy generation in similar nanowires using temperature-dependent steady-state photoluminescence, a phenomenon induced by strong exciton localization effects and charge carrier trapping by surface defect states.^{29,30} Our previous thermodynamic approach was utilized to provide qualitative comparison between two materials (namely, $\text{In}_{0.32}\text{Ga}_{0.68}\text{N}$ and $\text{Al}_{0.18}\text{Ga}_{0.82}\text{N}$) in terms of their luminescent refrigeration efficiencies. The quantity we termed “generated entropy” evolved with temperature, but because there is no scale, this evolution could be anywhere between vast and marginal. Thus, this approach is rendered unsuitable for the assessment of the effectiveness of and comparison between surface passivation procedures. Here, we quantify the surface passivation effects through the Heisenberg uncertainty principle

$$\Delta\mathcal{H}\Delta Q \geq \langle\Psi|\frac{1}{2i}[\hat{\mathcal{H}}, \hat{Q}]\Psi\rangle \quad (1)$$

where \mathcal{H} and Q are arbitrary noncommuting observables, by introducing a figure of merit that employs Heisenberg's fundamental limit $\hbar/2$, advancing our understanding of the assessment of the effectiveness of surface state passivation.

Based on Fermi's golden rule,³¹ the strength of radiative recombination is a multiple of the magnitude of the transition matrix element, a dimensionless quantity that is directly proportional to the square of the electron–hole wave function spatial overlap matrix element

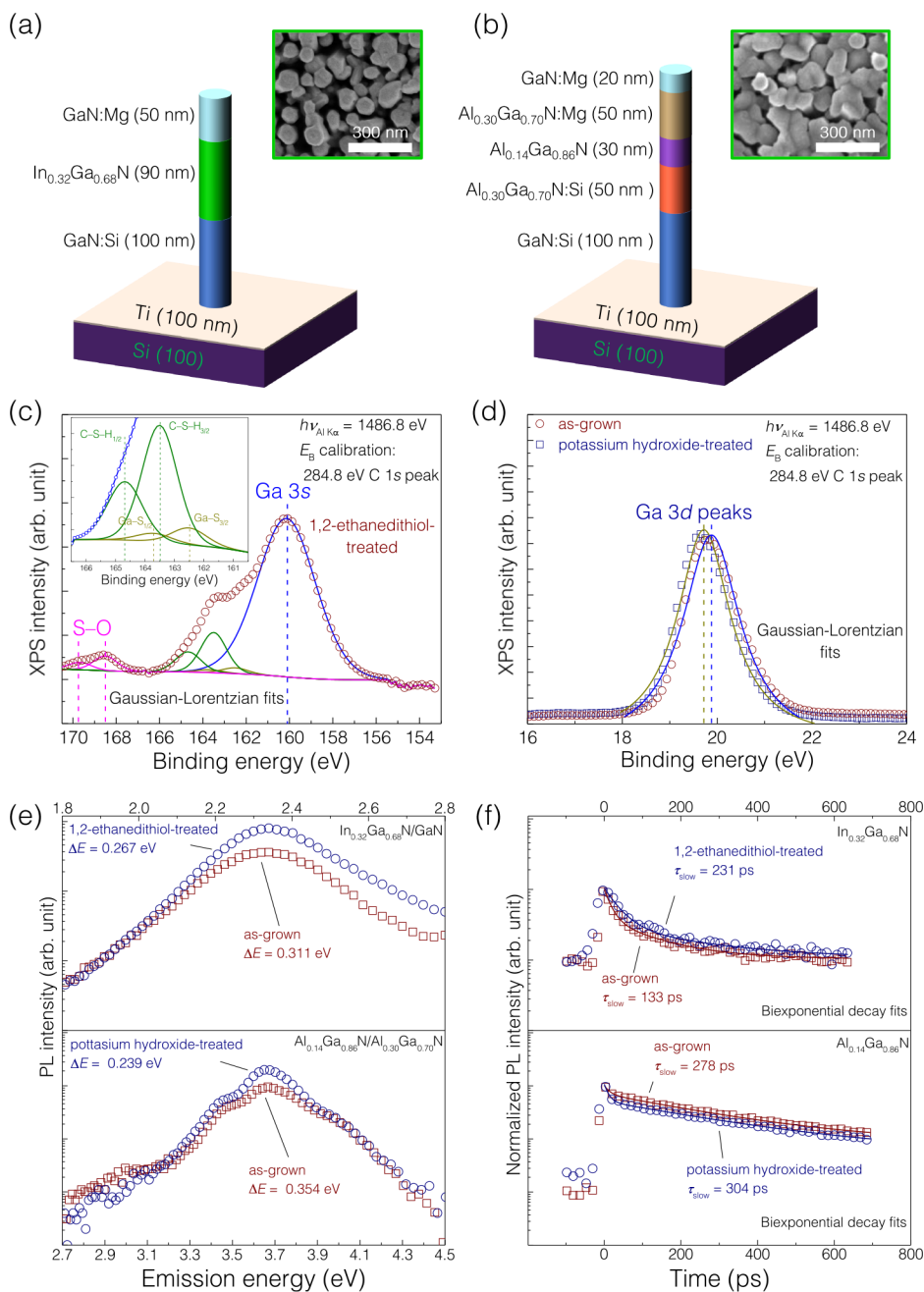


Figure 2. Simplified schematic and layer structures of an (a) $\text{In}_{0.32}\text{Ga}_{0.68}\text{N}/\text{GaN}$ double-heterostructure nanowire and (b) a multiquantum-disk $\text{Al}_{0.14}\text{Ga}_{0.86}\text{N}/\text{Al}_{0.30}\text{Ga}_{0.70}\text{N}$ nanowire. Insets: plan-view electron microscope images of the nanowire samples. (c) Fitted 1,2-ethanedithiol-treated Ga 3s/S 2p X-ray photoelectron spectrum from an ensemble of $\text{In}_{0.32}\text{Ga}_{0.68}\text{N}/\text{GaN}$ nanowires. Inset: zoomed-in view of the fitted 1,2-ethanedithiol-treated photoelectron spectrum. (d) Fitted potassium hydroxide-treated Ga 3d 2p X-ray photoelectron spectra from an ensemble of $\text{Al}_{0.14}\text{Ga}_{0.86}\text{N}/\text{Al}_{0.30}\text{Ga}_{0.70}\text{N}$ nanowires. (e) Semilogarithmic scale $\text{In}_{0.32}\text{Ga}_{0.68}\text{N}$ - and $\text{Al}_{0.14}\text{Ga}_{0.86}\text{N}/\text{Al}_{0.30}\text{Ga}_{0.70}\text{N}/\text{GaN}$ -related steady-state photoluminescence spectra before and after surface passivation showing homogeneous ($\text{In}_{0.32}\text{Ga}_{0.68}\text{N}$) and inhomogeneous ($\text{Al}_{0.14}\text{Ga}_{0.86}\text{N}/\text{Al}_{0.30}\text{Ga}_{0.70}\text{N}$) photon emission distributions at room temperature. (f) Semilogarithmic scale $\text{In}_{0.32}\text{Ga}_{0.68}\text{N}$ - and $\text{Al}_{0.14}\text{Ga}_{0.86}\text{N}$ -related as-grown and surface-treated time-resolved photoluminescence rise/decay curves at room temperature.

$$|\langle \Psi_h | \Psi_e \rangle|^2 = \left| \int_0^L dx \Psi_h^*(x) \Psi_e(x) \right|^2 \quad (2)$$

when written in terms of the inner product of the complex vector space of square-integrable functions $[0, L] \rightarrow \mathbb{C}$ with L being the one-dimensional (1D) spatial length of the quantum confined region. For an optical transition from a state of higher energy (Ψ_k) to a state of lower energy (Ψ_n), the optical

transition rate (W_{\downarrow}) caused by photoexcitation can be expressed as^{32,33}

$$W_{\downarrow} = \frac{2\pi}{\hbar} \sum_{n \neq k} \frac{|\langle \Psi_n | \hat{H}_{-} | \Psi_k \rangle|^2}{M_{k \rightarrow n}} \delta(\epsilon_k - \epsilon_n - \hbar\omega) \quad (3)$$

where $\hat{H}_{-} = H'(r, t) = -\frac{q}{m_0} \mathbf{A}(r, t) \cdot \mathbf{p}$ is the perturbation Hamiltonian of the downward optical transition $|\Psi_k\rangle \rightarrow |\Psi_n\rangle$ (where m_0 is the free electron mass, $\mathbf{A}(\mathbf{r}, t)$ is the vector

potential, and \mathbf{p} is the momentum operator). ε_k and ε_n are the energy eigenvalues of the eigenstates Ψ_k and Ψ_n , respectively. That being so, $\delta(\varepsilon_k - \varepsilon_n - \hbar\omega)$ in eq 3 is the Dirac delta function of an individual emission from a $k \rightarrow n$ transition that ensures energy conservation, whereas $M_{k \rightarrow n}$ is the square magnitude of the emission. The product of these two quantities, for each $n \neq k$, represents the selective emission for a particular transition. Nonetheless, in this work we stress the fact that quantifying the quality of molecular beam epitaxy (MBE)-grown nanowires incorporating only the $M_{k \rightarrow n}$ terms is insufficient. Indeed, with significant reduction in common impurities and vacancy centers, such as the growth-induced formation of carbon impurities^{34–36} and nitrogen-vacancy related defects,³⁷ surface recombination predominantly affects the performance of nanowire-based devices because the quantum efficiency of nanowire-based optoelectronic devices can be limited by the increased density of surface trap states (Shockley–Read–Hall recombination),³⁸ which also manifests itself by introducing lower-energy defect-induced photoemission because of band bending that distorts the shape of the photoemission spectrum as described earlier. The introduction of such emission centers can be accounted for by eq 3. Thus, we argue that incorporation of Heisenberg's uncertainty principle takes into account the dispersion behavior manifested by the delta terms in the optical transition rate W_{\downarrow} . As we examine the effectiveness of surface passivation in view of Heisenberg's uncertainty principle, we emphasize that deep-level traps within a direct bandgap can be created by defects in the material lattice structure whereby lattice vibration manifests itself in nonradiative interactions between phonons and defect channels in the material crystal structure.^{39,40}

2. NANOWIRE LAYER STRUCTURES AND SURFACE TREATMENT: METHODS

2.1. Nanowire Growth and Surface Passivation Protocols. As a test vehicle for our theoretical analysis, p–i–n nanowire heterostructures were grown by plasma-assisted MBE on titanium/TiN-coated silicon substrates, where the growth conditions are similar to what we reported previously for similarly synthesized samples.^{41,42} Titanium and TiN are excellent thermal conductors and therefore induce improved thermoelectric cooling characteristics compared to silicon, which aids in the enhancement of the luminescent refrigeration in optoelectronic devices.^{42,43} The direct growth of GaN-based nanowires on metal foils would avoid the complications of conventional transfer methods,⁴⁴ which significantly increases throughput while maintaining an excellent electrical contact to the nanowires.⁴⁵ Figures 2a and 2b show schematic illustrations of the double-heterostructure $\text{In}_{0.32}\text{Ga}_{0.68}\text{N}/\text{GaN}$ and partially coalesced $\text{Al}_{0.14}\text{Ga}_{0.86}\text{N}/\text{Al}_{0.30}\text{Ga}_{0.70}\text{N}$ nanowires examined here, with the c -axis along the growth directions normal to the substrates. With regards to one-dimensional quantum confinement effects, it is important to note that our nanowires are not ideal quantum nanowires as the cross-sectional sizes are relatively large when compared to the Bohr diameter of the three-dimensional excitons in their bulk counterpart, which is about 3 nm for GaN.⁴⁶ While the nanowires do not exhibit strong one-dimensional exciton quantum confinement effects, they do exhibit a center-of-mass confinement, leading to weak quantum confinement effects, which are still pronounced.

We started the surface passivation process of the $\text{In}_{0.32}\text{Ga}_{0.68}\text{N}/\text{GaN}$ nanowires by cleaning the sample with acetone and isopropyl alcohol. We then applied buffered-oxide-etch (BOE) solution for 45 s to remove any native oxide layers. After that, we immersed the sample in 1,2-ethanedithiol for 10 min to passivate the surfaces of the nanowires. We expected 1,2-ethanedithiol to reduce the $\text{In}_{0.32}\text{Ga}_{0.68}\text{N}/\text{GaN}$ surface state reaction sites, forming strong bonds between the sulfur and group III atoms, thereby terminating the dangling bonds at the nanowire sidewalls that trap charge carriers.^{11,13,14} We then cleaned the sample with ethanol. Likewise, after the $\text{Al}_{0.14}\text{Ga}_{0.86}\text{N}/\text{Al}_{0.30}\text{Ga}_{0.70}\text{N}$ nanowire growth, the nanowires were treated in a potassium hydroxide solution with a concentration of 10 wt % at 45 °C for 30 s. The nanowires were then rinsed in deionized water for 10 min. It was postulated and verified through macroscopic measurements that potassium hydroxide etches the nanowire surfaces, thereby reducing the dangling bonds.^{14,47} Evidence that confirm sidewall passivation action in nanowires with similar structure and nanowire density is demonstrated using high-resolution transmission electron microscopy (HRTEM) imaging in our previous publications.¹³ For photoluminescence characterization, the same sampled areas of the nanowires were characterized before and after surface passivation to ensure the consistency and comparability of the measurements.

2.2. Physical Evidence for Surface Passivation.

2.2.1. X-ray Photoelectron Spectroscopy Measurements. We investigated the change in surface chemical properties of the $\text{In}_{0.32}\text{Ga}_{0.68}\text{N}/\text{GaN}$ and $\text{Al}_{0.14}\text{Ga}_{0.86}\text{N}/\text{Al}_{0.30}\text{Ga}_{0.70}\text{N}$ nanowires after 1,2-ethanedithiol and potassium hydroxide surface passivation, respectively, by analyzing photoelectron spectroscopy results. High-resolution X-ray photoelectron spectroscopy (HRXPS) measurements were performed to analyze the surface properties of the nanowires before and after surface passivation. The photoelectron spectra were obtained with an Axis Ultra DLD system using an Al $K\alpha$ X-ray radiation source ($h\nu = 1486.8$ eV). The probing depth was ~ 10 nm with a measurement accuracy of ± 0.05 eV. The binding energy (E_B) was calibrated based on the 284.8 eV C 1s peak. The data analysis was performed with “CasaXPS”, and the peaks were fitted with a Gaussian–Lorentzian function. Because of discrepancies in the shapes of individual binding energy bands, spectral peaks were deconvoluted using a Gaussian–Lorentzian profile to extract the relevant elemental X-ray signatures. In Figure 2c, we show the Ga 3s/S 2p photoelectron spectrum for the 1,2-ethanedithiol-treated $\text{In}_{0.32}\text{Ga}_{0.68}\text{N}/\text{GaN}$ nanowire sample. The spectrum shows a peak at 160.6 eV corresponding to Ga 3s singlet. In addition, we show a zoomed-in view of the 1,2-ethanedithiol-treated photoelectron spectrum in the inset of Figure 2c, which was fitted with two (S 2p_{1/2}–S 2p_{3/2}) doublets. The two peaks centered at 163.4 and 164.6 eV (S 2p doublet) correspond to the C–S–H bond. An additional S 2p doublet located at 168.6 and 170.4 eV (Figure 2c) is attributed to the S–O bond from sulfur oxide formed after surface passivation.⁴⁸ In Figure 2d, we show the Ga 3d photoelectron spectra for the potassium hydroxide-treated $\text{Al}_{0.14}\text{Ga}_{0.86}\text{N}/\text{Al}_{0.30}\text{Ga}_{0.70}\text{N}$ nanowire sample before and after surface passivation. This passivation process was implemented effectively as the binding energy value of Ga 3d became smaller after surface treatment (decreased from 19.9 to 19.6 eV), indicating the considerable termination of the surface dangling bonds and removal of surface oxides.^{49–51}

2.2.2. Steady-State and Transient Photoluminescence Measurements. The surface passivation effects are also evident from the steady-state and transient photoluminescence spectra of the nanowires at room temperature. The photoluminescence measurements were performed with a mode-locked Ti:sapphire laser (Coherent Mira 900) having a laser power output of 1.90 W at 800 nm, and the measurements were used to study the photoemission energy dispersion and carrier lifetimes in the active layers of the nanowires. A third harmonic generator (APE-SHG/THG) was used to excite the sample by an output wavelength (λ_{ex}) of 266 nm at room temperature. Emission of the samples was detected by a monochromator attached to a UV-sensitive Hamamatsu C6860 streak camera with a temporal resolution of 2 ps. We fitted the steady-state photoluminescence spectra with Cauchy–Lorentz distributions to extract the emission line widths as discussed in the [Supporting Information](#). The transient photoluminescence decay curves were fitted and analyzed by using a biexponential decay model, which provided the most proper fit because of the multicenter recombination characteristics exhibited by the nanowires.^{14,29,30,52} Figures 2e and 2f show the $\text{In}_{0.32}\text{Ga}_{0.68}\text{N}$ - and $\text{Al}_{0.14}\text{Ga}_{0.86}\text{N}/\text{Al}_{0.30}\text{Ga}_{0.70}\text{N}$ -related steady-state and transient photoluminescence spectra, respectively, of the samples before and after the 1,2-ethanedithiol and potassium hydroxide passivation. We observe the reduction in energy dispersion after surface passivation, from $\Delta E = 0.311$ to 0.267 eV for $\text{In}_{0.32}\text{Ga}_{0.68}\text{N}$ and $\Delta E = 0.354$ to 0.239 eV for $\text{Al}_{0.14}\text{Ga}_{0.86}\text{N}/\text{Al}_{0.30}\text{Ga}_{0.70}\text{N}$, implying reduced carrier recombination at defect centers.

On the other hand, because nonradiative recombination channels can dominate the excitonic recombination processes at room temperature,^{11,29} we observe slower recombination lifetimes of $\tau_{\text{slow}} = 231$ ps in $\text{In}_{0.32}\text{Ga}_{0.68}\text{N}$ and $\tau_{\text{slow}} = 304$ ps in $\text{Al}_{0.14}\text{Ga}_{0.86}\text{N}$ subsequent to surface passivation compared to 133 and 278 ps, respectively, prior to surface passivation, indicating that the surface treatment protocols had reduced the density of surface defect states and significantly recovered the band-edge emission as longer nonradiative recombination lifetimes are a signature of the suppression of surface states.^{22,53,54} Subsequent to the surface passivation, the peak spectral intensities of $\text{Al}_{0.14}\text{Ga}_{0.86}\text{N}$ - and $\text{In}_{0.32}\text{Ga}_{0.68}\text{N}$ -related photoluminescence emission increased more than 2- and 3-fold, respectively, in linear scale. The enhancement in the spectral peak intensities is attributed to the effective surface passivation using 1,2-ethanedithiol and potassium hydroxide, which synchronously reduced surface states and recovered the band-edge emission, leading to a reduction in the surface recombination velocity (S, see the [Supporting Information](#)) because of the higher density of nonradiative recombination channel at room temperature and an increase in the photoluminescence peak spectral intensity.

3. DERIVATION OF A SURFACE PASSIVATION FIGURE OF MERIT

Herein, we undertake to determine an approximation of the degree of dispersion in observed carrier relaxation lifetimes and recovery of band-edge emission of atomic transitions after nanowire surface state passivation as measured using steady state and transient photoluminescence at room temperature.

3.1. Derivation of Dispersion in Carrier Lifetime and Emission Energy Relations. We recall the classical form of Heisenberg's uncertainty principle that relates the measure-

ment of the dispersion in time (t) and energy (\mathcal{E}) for an excited atom

$$\Delta t \Delta \mathcal{E} \geq \frac{\hbar}{2} \quad (4)$$

where $\Delta t = \tau$ and $\Delta \mathcal{E}$ resembles the uncertainty in time and energy, respectively, that are arising from wave properties inherent in the quantum mechanical wave–particle nature of a measured system.⁵⁵ Whenever an atom undergoes a downward transition between electronic states, quantized amounts of energy are released in the form of photons, each of which has a radiation frequency (ω_n) that is associated with its energy ($\mathcal{E}_n^{\text{ph}}$) by $\mathcal{E}_n^{\text{ph}}(\omega_n) = \hbar\omega_n$ ($n \in \mathbb{N}$ being the photon number). The average time interval after excitation during which an atom radiates is termed the effective decay lifetime ($\Delta t = \tau_{\text{avg}}$ ^{56,57}), which we took as τ_{slow} (inferred from fitted biexponential decay models in our time-resolved photoluminescence experiments).²⁹ Unlike the measurement of two conjugate variables with noncommuting operators, say a particle's position \hat{r} and its associated momentum \hat{p} , whose canonical commutator relation is $[\hat{r}_k, \hat{p}_n] = i\hbar\delta_{kn} = 0$ for $k \neq n$, $\hat{\mathcal{E}}$ and t cannot satisfy a canonical commutation relation because t is not a Hermitian operator; rather, it is a nondynamic independent variable on which the dynamical variable \mathcal{E} —represented by its corresponding operator $\hat{\mathcal{E}}$ —is dependent.^{55,58,59} Uncertainty in measured \mathcal{E} (Figure 3) is

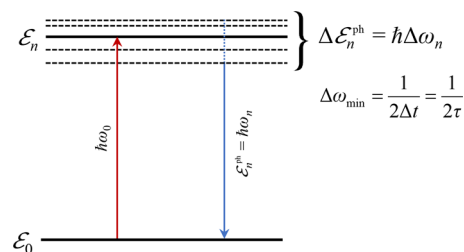


Figure 3. Illustration of the uncertainty in measured \mathcal{E} during the decay from excited states in a measured system.

what we observe during the decay from excited states, when, for example, measured by time-resolved spectroscopy techniques.^{60,61} If $\Delta \mathcal{E} \rightarrow 0$, then $\tau \rightarrow \infty$, implying that the system would permanently remain in its stationary state. However, the system decays because the excited levels are not stationary (e.g., they can be a linear overlap of different eigenstates). In this case, the state is an overlap of stationary states ($\Psi = \sum a_m \Psi_m$) that are not eigenstates of the Hamiltonian ($\hat{H}\Psi \neq \mathcal{E}\Psi$).⁵⁶ This results in $\Delta \mathcal{E} \neq 0$ and a finite nonzero Δt . As a consequence, the emitted photons have an energy uncertainty $\hbar\Delta\omega$ because of finite Δt . Therefore, for typical steady-state and transient photoluminescence measurements, the uncertainty principle can be stated as

$$\tau \Delta \mathcal{E}_\nu(\omega_n) \geq \frac{\hbar}{2} \quad (5)$$

where τ is taken as the effective relaxation time that was observed over certain emission energy/wavelength window, and $\Delta \mathcal{E}_\nu(\omega_n)$ is the dispersion in photon energy emission as measured within the same window during which τ was averaged. This uncertainty corresponds to a minimum uncertainty in ω through the Heisenberg uncertainty principle.

We necessarily note that these uncertainty arise from the quantum structure of the layered materials comprising the nanowires, including perturbative defects embedded in the crystalline material such as local defects and surface states, not the photoluminescence measurement process itself.⁶² This form of the uncertainty principle given in eq 5 may imply that energy conservation can appear to be violated by an amount $\Delta\mathcal{E}_\nu = \hbar \int d\omega$ (taking into account the dispersion in photon energies).⁵⁷ Here, we propose a bound within which the degree of surface state passivation can be restricted that relies strictly on the photoluminescent emission's dispersion in energy and lifetime. As a result of the recovery of band-edge emission and the carrier lifetime dispersion after surface passivation (say, at room temperature), we have

$$\tau_\alpha < \tau_\beta \quad (6)$$

$$(\Delta\mathcal{E}_\nu(\omega_n))_\alpha > (\Delta\mathcal{E}_\nu(\omega_n))_\beta \quad (7)$$

where τ_α and τ_β are the effective measured carrier lifetimes, as defined in eq 5, before and after surface passivation, respectively. Analogously, $(\Delta\mathcal{E}_\nu(\omega_n))_\alpha$ and $(\Delta\mathcal{E}_\nu(\omega_n))_\beta$ are the dispersion in emission energy before and after passivation, respectively. To deduce a limit that improves on Heisenberg's uncertainty limit $\hbar/2$, we define a set of four parameters (hereafter termed the *four deltas*) as follows:

$$\Delta_\alpha = \tau_\alpha(\Delta\mathcal{E}_\nu(\omega_n))_\alpha \geq \frac{\hbar}{2} \quad (8)$$

$$\Delta_\beta = \tau_\beta(\Delta\mathcal{E}_\nu(\omega_n))_\beta \geq \frac{\hbar}{2} \quad (9)$$

$$\Delta_\gamma = \tau_\alpha(\Delta\mathcal{E}_\nu(\omega_n))_\beta \quad (10)$$

$$\Delta_\varepsilon = \tau_\beta(\Delta\mathcal{E}_\nu(\omega_n))_\alpha \quad (11)$$

where Δ_α and Δ_β are absolute and Δ_γ and Δ_ε are mixed deltas. We will assume that strict inequalities occur in both eqs 8 and 9. From eqs 6 and 7, we infer the following inequalities

$$\Delta_\varepsilon > \Delta_\beta > \Delta_\gamma \quad (12)$$

$$\Delta_\varepsilon > \Delta_\alpha > \Delta_\gamma \quad (13)$$

So, $(\Delta_\gamma, \Delta_\varepsilon)$ is a nonempty interval containing both Δ_α and Δ_β

$$\Delta_\alpha, \Delta_\beta \in (\Delta_\gamma, \Delta_\varepsilon) \quad (14)$$

Furthermore, we cannot a priori compare Δ_α and Δ_β but by Heisenberg's uncertainty principle we know that both Δ_α and Δ_β cannot fall below $\hbar/2$. In other words, Heisenberg's uncertainty principle applied for our system before and after passivation can be restated as

$$\Delta_\alpha, \Delta_\beta \in \left(\frac{\hbar}{2}, \infty\right) \quad (15)$$

If $(\Delta\mathcal{E}_\nu(\omega_n))_\alpha - (\Delta\mathcal{E}_\nu(\omega_n))_\beta$ is infinitesimally small, then Δ_γ will exceed $\hbar/2$

$$\Delta_\gamma > \frac{\hbar}{2} \quad (16)$$

Thus, we have the strict inclusion

$$(\Delta_\gamma, \infty) \subset \left(\frac{\hbar}{2}, \infty\right) \quad (17)$$

So, knowledge of $(\Delta\mathcal{E}_\nu(\omega_n))_\beta$ alone allows one to calculate Δ_γ and would supposedly improve on the Heisenberg uncertainty principle in view of eq 12. Likewise, when $\tau_\beta - \tau_\alpha$ is infinitesimally small, Δ_γ will exceed $\hbar/2$ and we obtain the same conclusion; that is

$$\Delta_\gamma > \frac{\hbar}{2}$$

3.2. Deduction of a Passivation Metric. Given a set of information represented as a conjunction of logical statements and observations, \mathcal{I} , we define $l(\mathcal{I})$ as the greatest lower bound that one can prove on Δ_β . As applying the Heisenberg uncertainty principle to our system after passivation yields a lower bound on Δ_β , namely, $\hbar/2$, letting \mathcal{I}_0 denote a fixed minimal conjunction of statements allowing the derivation of Heisenberg's uncertainty principle one would obtain

$$l(\mathcal{I}_0) = \frac{\hbar}{2} \quad (18)$$

by the tightness of the isoperimetric inequality. Of course, letting D be the statement that we have measured Δ_β , then with

$$\mathcal{I}_1 := D \wedge \mathcal{I}_0 \quad (19)$$

we would have

$$l(\mathcal{I}_1) = \Delta_\beta \quad (20)$$

In addition, for any \mathcal{I}

$$l(\mathcal{I}) \leq \Delta_\beta \quad (21)$$

Letting E be the statement that we measured τ_α and $(\Delta\mathcal{E})_\beta$, then with

$$\mathcal{I}_2 := E \wedge \mathcal{I}_0 \quad (22)$$

we have that

$$l(\mathcal{I}_2) \geq \max\left(\Delta_\gamma, \frac{\hbar}{2}\right) \quad (23)$$

We use the lower bound $\max\left(\Delta_\gamma, \frac{\hbar}{2}\right)$ as a proxy for $l(\mathcal{I}_2)$. This assumption is justified by the fact that knowledge of the energy dispersion (after passivation) does not indicate the amount of the dispersion in carrier lifetime (after passivation), for one does not know where the peak energy emission is located (e.g., red- or blue-shifts could occur).

While there is a wide range of possibilities, and we can determine the four deltas after surface passivation, the lower bound obtained on Δ_β via l by considering Δ_γ for a passivation that does not significantly change the energy dispersion is a lower limit that improves on Heisenberg's uncertainty principle. On the other hand, we should not get an easy improvement on Heisenberg's uncertainty principle, meaning that if this number is not lower than the lower limit of Heisenberg's, then we could claim that the material after passivation did not undergo dangling bond termination, so the passivation quality is poor. Furthermore, in the limit where there is no passivation, the four deltas collapse as they become equal to one another (i.e., $\Delta_\alpha = \Delta_\beta = \Delta_\gamma = \Delta_\varepsilon$). In this limit, we will have $\Delta_\gamma/\Delta_\varepsilon = 1$. When passivation effects occur, the ratio $\Delta_\gamma/\Delta_\varepsilon$ will become less than one. The closer this ratio to zero, the better the passivation. Put differently, the lower the ratio, the larger the interval bounded by Δ_γ and Δ_ε .

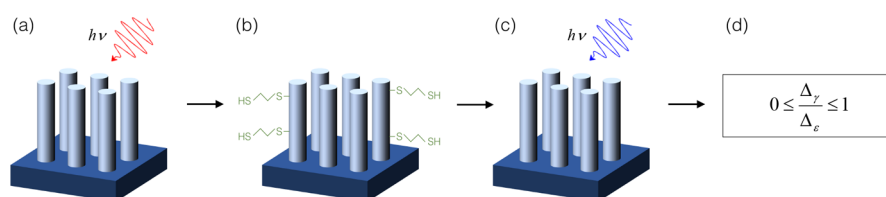


Figure 4. Graphical summary of our experimental method and analysis: (a) performing steady-state and transient photoluminescence measurements prior to surface passivation, (b) applying a surface passivation protocol, (c) performing steady-state and transient photoluminescence measurements after surface passivation, and (d) calculating Δ_γ and Δ_ϵ to determine the effectiveness of the surface passivation protocol.

Table 1. Summary of the Assessed Surface Passivation Goodness for the Materials and Passivation Protocols Discussed in This Article^a

material	$(\Delta\mathcal{E}_\nu(\omega_n))_\alpha$	$(\Delta\mathcal{E}_\nu(\omega_n))_\beta$	τ_α	τ_β	Δ_γ	Δ_ϵ	$\Delta_\gamma/\Delta_\epsilon$
$\text{In}_{0.32}\text{Ga}_{0.68}\text{N}$	0.311	0.267	133	231	3.55	7.18	0.49
$\text{Al}_{0.14}\text{Ga}_{0.86}\text{N}$	0.354	0.239	278	304	6.64	10.76	0.62

^aBoth passivations have moderate effects as their calculated $\Delta_\gamma/\Delta_\epsilon$ ratios lie in or close to the middle of the interval defined in eq 24. As the $\Delta_\gamma/\Delta_\epsilon$ ratio is smaller for $\text{In}_{0.32}\text{Ga}_{0.68}\text{N}$, the passivation is more salient than for $\text{Al}_{0.14}\text{Ga}_{0.86}\text{N}$. $(\Delta\mathcal{E}_\nu(\omega_n))_\alpha$ and $(\Delta\mathcal{E}_\nu(\omega_n))_\beta$ are expressed in eV, and τ_α and τ_β are expressed in ps, whereas Δ_γ and Δ_ϵ are expressed in 10^{-11} eV·s.

$$0 \leq \frac{\Delta_\gamma}{\Delta_\epsilon} \leq 1 \quad (24)$$

while we have

$$\Delta_\gamma \ll \Delta_\beta \rightarrow \tau_\beta \text{ is higher}$$

$$\Delta_\epsilon \gg \Delta_\beta \rightarrow (\Delta\mathcal{E})_\beta \text{ is lower}$$

Figure 4 depicts a graphical summary of our experimental method and analysis. The method and analysis presented here can be applied to other forms of direct bandgap semiconductor materials. Our model relies solely on the dispersion in energy and lifetime of electron–hole recombination emission at room temperature. In addition to our quasi-1D nanowires, the model can be extended other forms of nanostructures such as thin films (Figure 4 depicts nanowires for illustration purposes only).

4. DISCUSSION AND ANALYSIS

The limit $l(I_2) \rightarrow \hbar/2$ signifies having more information about the goodness of the passivation protocol in virtue of us having less information about the current state of the material surfaces, given their previous state prior to implementing the passivation protocol. What is more, if we only measure τ_α and $(\Delta\mathcal{E}_\nu(\omega_n))_\beta$ we establish a figure of merit by comparing Δ_γ to Heisenberg's limit $\hbar/2$, based on the fact that we have less information:

1. $\Delta_\gamma \gg \hbar/2$: Given the original state of the material surface, we still know a great deal about the material surface condition after surface passivation, indicating a *null* passivation of the material surface dangling bonds.
2. $\Delta_\gamma > \hbar/2$: The knowledge we acquired indicates a *moderate* passivation of surface defect states.
3. $\Delta_\gamma < \hbar/2$: More knowledge is lost about the new state of the material, indicating a *good* passivation of surface defect states.
4. $\Delta_\gamma \ll \hbar/2$: We know practically nothing about the new state of the material surface, indicating practically *ideal* passivation from a photoluminescent point of view,

because Δ_γ is in this case a noninformative lower bound on Δ_β .

Table 1 summarizes our experimental results from this paper. The calculated values of Δ_γ for $\text{In}_{0.32}\text{Ga}_{0.68}\text{N}$ and $\text{Al}_{0.14}\text{Ga}_{0.86}\text{N}$ are 3.55 and 6.64×10^{-11} eV·s, respectively. Given that $\hbar/2 = h/4\pi \approx 6.58 \times 10^{-16}$ eV·s, we have $\Delta_\gamma/(\hbar/2) \approx 5.40 \times 10^4$ for $\text{In}_{0.32}\text{Ga}_{0.68}\text{N}$ and $\approx 1.01 \times 10^5$ eV·s for $\text{Al}_{0.14}\text{Ga}_{0.86}\text{N}$. Figure 5 demonstrates a graphical depiction of the different qualities inferred about the passivation goodness from the size of Δ_γ . Thus, Δ_γ has the significance of telling us the largest lower bound on Δ_β . In other words, when we determine Δ_γ , we ascertain whether it is very close to Δ_β . If so, then the passivation did not significantly alter the material surface and would not enhance its photoluminescence performance. Then we take the ratio $\Delta_\gamma/\Delta_\epsilon$, whose shrinkage correlates with more effective surface state passivation. The closer the ratio is to unity, the closer the material surface is to its original state.

5. CONCLUDING REMARKS AND FUTURE WORK

In summary, we proposed a method to quantify the effectiveness of nanowire surface passivation protocols in terms of the quantum uncertainty lower bound. In particular, the methodology developed and discussed here takes into account the change in the effective carrier lifetime and energy dispersion of a photoluminescent system. By correlating the extracted carrier lifetimes and photon energy dispersion values from steady-state and transient photoemission responses, respectively, the degree of enhancement in radiative recombination in ensembles of semiconductor nanowires after surface treatment was quantified within a derived limit ($\Delta_\gamma/\Delta_\epsilon \in [0, 1]$). By generalizing the uncertainty principle to our photoluminescence measurements of nanowires, we were able to define a strict limit and introduce an indicator of the effectiveness of surface passivation protocols. Ideally, if we have two similar samples of nanostructured semiconductor materials and we perform two different surface passivation experiments, we will aim to find out which one produces higher Δ_ϵ and lower Δ_γ values, but the way we demonstrate the goodness of surface state passivation here gives us another view

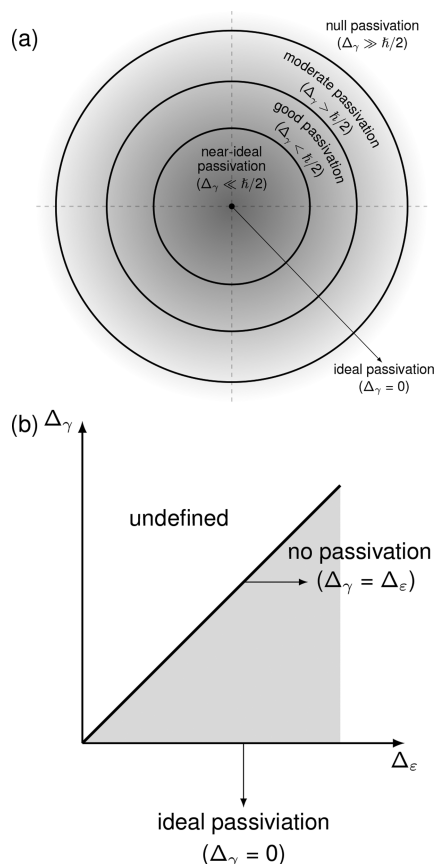


Figure 5. A graphical illustration of the different qualities inferred about the passivation goodness from the size of Δ_γ : (a) Δ_γ relation to $\hbar/2$; (b) Δ_γ relation to Δ_ϵ .

on why lower Δ_γ is better. Namely, when Δ_γ is lower, the material is becoming less like that before passivation in virtue of the enhancement of optoelectronic properties of the passivated nanostructure surfaces.

As is the case with novel measures of effectiveness, the extreme cases are usually clearer than the gradient in between. For instance, we argued that if our passivation figure of merit (cf. eq 24) being equal to zero or unity corresponds to ideal or completely nonexistent passivation, respectively. Further research could investigate whether, for the intermediate regime, inferred effectiveness grows linearly or otherwise as a function of the $\Delta_\gamma/\Delta_\epsilon$. Finally, surfactants significantly reduce the surface tension of the chemical passivation agent. While the use of surfactants in a highly dense nanowire ensemble was not discussed in the present work, the utilization of surfactants could ensure a more effective passivation of nanowire surfaces in such nanowire ensembles. Extending our work to incorporate the effect of surfactants would further the understanding of the extent of passivation effectiveness by developing more quantitative analyses and benchmarking our model.

■ ASSOCIATED CONTENT

Supporting Information

The Supporting Information is available free of charge at <https://pubs.acs.org/doi/10.1021/acsaelm.9b00578>.

Spectral peak fitting, surface recombination, and conventional passivation performance metrics (PDF)

■ AUTHOR INFORMATION

Corresponding Authors

Nasir Alfaraj – King Abdullah University of Science and Technology (KAUST), Thuwal 23955-6900, Saudi Arabia; orcid.org/0000-0002-0429-9439; Email: nasir.alfaraj@kaust.edu.sa

Xiaohang Li – King Abdullah University of Science and Technology (KAUST), Thuwal 23955-6900, Saudi Arabia; orcid.org/0000-0002-4434-365X; Email: xiaohang.li@kaust.edu.sa

Other Authors

Wael Alghamdi – Harvard University, Cambridge, Massachusetts 02138, United States

Meshal Alaweini – University of California, Berkeley, Berkeley, California 94720, United States

Idris A. Ajia – King Abdullah University of Science and Technology (KAUST), Thuwal 23955-6900, Saudi Arabia

Daive Priante – King Abdullah University of Science and Technology (KAUST), Thuwal 23955-6900, Saudi Arabia

Bilal Janjua – King Abdullah University of Science and Technology (KAUST), Thuwal 23955-6900, Saudi Arabia

Haiding Sun – King Abdullah University of Science and Technology (KAUST), Thuwal 23955-6900, Saudi Arabia

Tien Khee Ng – King Abdullah University of Science and Technology (KAUST), Thuwal 23955-6900, Saudi Arabia; orcid.org/0000-0002-1480-6975

Boon S. Ooi – King Abdullah University of Science and Technology (KAUST), Thuwal 23955-6900, Saudi Arabia

Iman S. Roqan – King Abdullah University of Science and Technology (KAUST), Thuwal 23955-6900, Saudi Arabia; orcid.org/0000-0001-7442-4330

Complete contact information is available at:

<https://pubs.acs.org/doi/10.1021/acsaelm.9b00578>

Author Contributions

[†]N.A. and W.A. equally contributed to this work.

Notes

The authors declare no competing financial interest.

■ ACKNOWLEDGMENTS

This publication is based upon work supported by the King Abdullah University of Science and Technology (KAUST) baseline funding, BAS/1/1664-01-01, Competitive Research Grant (CRG) URF/1/3437-01-01 and URF/1/3771-01-01, and GCC Research Council Grant REP/1/3189-01-01. D.P., B.J., T.K.N., and B.S.O. acknowledge the financial support from King Abdulaziz City for Science and Technology (KACST), Grant KACST TIC R2-FP-008, KAUST baseline funding, BAS/1/1614-01-01, and MBE equipment funding, C/M-20000-12-001-77. The authors thank Prof. Enzo Di Fabrizio of KAUST for his helpful suggestions and insightful comments on the manuscript.

■ REFERENCES

- (1) Zhang, Z.; Yates, J. T., Jr. Band Bending in Semiconductors: Chemical and Physical Consequences at Surfaces and Interfaces. *Chem. Rev.* **2012**, *112*, 5520–5551.
- (2) Zhou, X. T.; Heigl, F.; Murphy, M. W.; Sham, T. K.; Regier, T.; Coulthard, I.; Blyth, R. I. R. Time-Resolved X-Ray Excited Optical Luminescence from SnO₂ Nanoribbons: Direct Evidence for the Origin of the Blue Luminescence and the Role of Surface States. *Appl. Phys. Lett.* **2006**, *89*, 213109.

- (3) Heine, V. Theory of Surface States. *Phys. Rev.* **1965**, *138*, A1689.
- (4) Alfaraj, N.; Min, J.-W.; Kang, C. H.; Alatawi, A. A.; Priante, D.; Subedi, R. C.; Tangi, M.; Ng, T. K.; Ooi, B. S. Deep-Ultraviolet Integrated Photonic and Optoelectronic Devices: A Prospect of the Hybridization of Group III–Nitrides, III–Oxides, and Two-Dimensional Materials. *J. Semicond.* **2019**, *40*, 121801.
- (5) Ren, D.; Azizur-Rahman, K. M.; Rong, Z.; Juang, B.-C.; Somasundaram, S.; Shahili, M.; Farrell, A. C.; Williams, B.; Huffaker, D. L. Room-Temperature Mid-Wavelength Infrared InAsSb Nanowire Photodetector Arrays with Al₂O₃ Passivation. *Nano Lett.* **2019**, *19*, 2793–2802.
- (6) Ren, D.; Scofield, A. C.; Farrell, A. C.; Rong, Z.; Haddad, M. A.; Laghumavarapu, R. B.; Liang, B.; Huffaker, D. L. Exploring Time-Resolved Photoluminescence for Nanowires Using a Three-Dimensional Computational Transient Model. *Nanoscale* **2018**, *10*, 7792–7802.
- (7) Ren, D.; Rong, Z.; Somasundaram, S.; Azizur-Rahman, K. M.; Liang, B.; Huffaker, D. L. A Three-Dimensional Insight into Correlation Between Carrier Lifetime and Surface Recombination Velocity for Nanowires. *Nanotechnology* **2018**, *29*, 504003.
- (8) Almutlaq, J.; Yin, J.; Mohammed, O. F.; Bakr, O. M. The Benefit and Challenges of Zero-Dimensional Perovskites. *J. Phys. Chem. Lett.* **2018**, *9*, 4131–4138.
- (9) Khan, J. I.; Adhikari, A.; Sun, J.; Priante, D.; Bose, R.; Shaheen, B. S.; Ng, T. K.; Zhao, C.; Bakr, O. M.; Ooi, B. S.; Mohammed, O. F. Enhanced Optoelectronic Performance of a Passivated Nanowire-Based Device: Key Information from Real-Space Imaging Using 4D Electron Microscopy. *Small* **2016**, *12*, 2313–2320.
- (10) Bose, R.; Sun, J.; Khan, J. I.; Shaheen, B. S.; Adhikari, A.; Ng, T. K.; Burlakov, V. M.; Parida, M. R.; Priante, D.; Goriely, A.; Ooi, B. S.; Bakr, O. M.; Mohammed, O. F. Real-Space Visualization of Energy Loss and Carrier Diffusion in a Semiconductor Nanowire Array Using 4D Electron Microscopy. *Adv. Mater.* **2016**, *28*, 5106–5111.
- (11) Zhao, C.; Ng, T. K.; Prabaswara, A.; Conroy, M.; Jahangir, S.; Frost, T.; O'Connell, J.; Holmes, J. D.; Parbrook, P. J.; Bhattacharya, P.; Ooi, B. S. An Enhanced Surface Passivation Effect in InGaN/GaN Disk-in-Nanowire Light Emitting Diodes for Mitigating Shockley–Read–Hall Recombination. *Nanoscale* **2015**, *7*, 16658–16665.
- (12) Majid, S.; Ruegg, H. Bicosproduct Structure of κ -Poincaré Group and Noncommutative Geometry. *Phys. Lett. B* **1994**, *334*, 348–354.
- (13) Varadhan, P.; Fu, H.-C.; Priante, D.; Retamal, J. R. D.; Zhao, C.; Ebaid, M.; Ng, T. K.; Ajia, I.; Mitra, S.; Roqan, I. S.; Ooi, B. S.; He, J.-H. Surface Passivation of GaN Nanowires for Enhanced Photoelectrochemical Water-Splitting. *Nano Lett.* **2017**, *17*, 1520–1528.
- (14) Sun, H.; Shakfa, M. K.; Muhammed, M. M.; Janjua, B.; Li, K.-H.; Lin, R.; Ng, T. K.; Roqan, I. S.; Ooi, B. S.; Li, X. Surface-Passivated AlGaIn Nanowires for Enhanced Luminescence of Ultraviolet Light Emitting Diodes. *ACS Photonics* **2018**, *5*, 964–970.
- (15) Han, D.; Ma, S.; Jia, Z.; Liu, P.; Jia, W.; Shang, L.; Zhai, G.; Xu, B. Morphologies and Optical and Electrical Properties of InGaIn/GaN Micro-Square Array Light-Emitting Diode Chips. *Appl. Opt.* **2018**, *57*, 2835–2840.
- (16) Ferrari, L.; Smalley, J. S.; Qian, H.; Tanaka, A.; Lu, D.; Dayeh, S.; Fainman, Y.; Liu, Z. Design and Analysis of Blue InGaIn/GaN Plasmonic LED for High-Speed, High-Efficiency Optical Communications. *ACS Photonics* **2018**, *5*, 3557–3564.
- (17) Gao, H.; et al. Optical Signatures of Deep Level Defects in Ga₂O₃. *Appl. Phys. Lett.* **2018**, *112*, 242102.
- (18) Mattila, T.; Nieminen, R. M. Point-Defect Complexes and Broadband Luminescence in GaN and AlN. *Phys. Rev. B: Condens. Matter Mater. Phys.* **1997**, *55*, 9571–9576.
- (19) Huang, Y.; Duan, X.; Cui, Y.; Lieber, C. M. Gallium Nitride Nanowire Nanodevices. *Nano Lett.* **2002**, *2*, 101–104.
- (20) Wang, Z.; Hao, Z.; Yu, J.; Wang, L.; Wang, J.; Sun, C.; Xiong, B.; Han, Y.; Li, H.; Luo, Y. Surface-Induced Carrier Localization and Recombination Characteristics in InGaIn/GaN Quantum Dots in Nanopillars. *J. Phys. Chem. C* **2019**, *123*, 5699–5704.
- (21) Deshpande, S.; Das, A.; Bhattacharya, P. Blue Single Photon Emission up to 200 K from an InGaIn Quantum Dot in AlGaIn Nanowire. *Appl. Phys. Lett.* **2013**, *102*, 161114.
- (22) Sun, M. H.; Joyce, H. J.; Gao, Q.; Tan, H. H.; Jagadish, C.; Ning, C.-Z. Removal of Surface States and Recovery of Band-Edge Emission in InAs Nanowires through Surface Passivation. *Nano Lett.* **2012**, *12*, 3378–3384.
- (23) Alia, S. M.; Duong, K.; Liu, T.; Jensen, K.; Yan, Y. Supportless Silver Nanowires as Oxygen Reduction Reaction Catalysts for Hydroxide-Exchange Membrane Fuel Cells. *ChemSusChem* **2012**, *5*, 1619–1624.
- (24) Rao, V. G.; Aslam, U.; Linic, S. Chemical Requirement for Extracting Energetic Charge Carriers from Plasmonic Metal Nanoparticles to Perform Electron-Transfer Reactions. *J. Am. Chem. Soc.* **2019**, *141*, 643–647.
- (25) Wu, K.; Chen, J.; McBride, J. R.; Lian, T. Efficient Hot-Electron Transfer by a Plasmon-Induced Interfacial Charge-Transfer Transition. *Science* **2015**, *349*, 632–635.
- (26) Haug, T.; Klemm, P.; Bange, S.; Lupton, J. M. Hot-Electron Intraband Luminescence from Single Hot Spots in Noble-Metal Nanoparticle Films. *Phys. Rev. Lett.* **2015**, *115*, 067403.
- (27) Pershoguba, S. S.; Yakovenko, V. M. Shockley Model Description of Surface States in Topological Insulators. *Phys. Rev. B: Condens. Matter Mater. Phys.* **2012**, *86*, 075304.
- (28) Shockley, W. On the Surface States Associated with a Periodic Potential. *Phys. Rev.* **1939**, *56*, 317.
- (29) Alfaraj, N.; Mitra, S.; Wu, F.; Ajia, I. A.; Janjua, B.; Prabaswara, A.; Aljefri, R. A.; Sun, H.; Ng, T. K.; Ooi, B. S.; Roqan, I. S.; Li, X. Photoinduced Entropy of InGaIn/GaN p-i-n Double-Heterostructure Nanowires. *Appl. Phys. Lett.* **2017**, *110*, 161110.
- (30) Alfaraj, N.; Muhammed, M. M.; Li, K.-H.; Janjua, B.; Aljefri, R. A.; Sun, H.; Ng, T. K.; Ooi, B. S.; Roqan, I. S.; Li, X. Thermodynamic Photoinduced Disorder in AlGaIn Nanowires. *AIP Adv.* **2017**, *7*, 125113.
- (31) Fermi, E. *Nuclear Physics: A Course Given by Enrico Fermi at the University of Chicago*; University of Chicago Press: 1950.
- (32) Wang, Z.; Currie, M.; Dianat, P.; Montazeri, K.; Nabat, B. Enhancement of Optoelectronic Properties of Core–Shell Nanowires. *IEEE Trans. Nanotechnol.* **2018**, *17*, 1058–1062.
- (33) Kevan, S. D.; Eberhardt, W. *Stud. Surf. Sci. Catal.* **1992**, *74*, 99–143.
- (34) Zhao, C.; Alfaraj, N.; Subedi, R. C.; Liang, J. W.; Alatawi, A. A.; Alhamoud, A. A.; Ebaid, M.; Alias, M. S.; Ng, T. K.; Ooi, B. S. III-Nitride Nanowires on Unconventional Substrates: From Materials to Optoelectronic Device Applications. *Prog. Quantum Electron.* **2018**, *61*, 1–31.
- (35) Sun, H.; Wu, F.; Al tahtamouni, T. M.; Alfaraj, N.; Li, K.-H.; Detchprohm, T.; Dupuis, R. D.; Li, X. Structural Properties, Crystal Quality and Growth Modes of MOCVD-Grown AlN with TMAI Pretreatment of Sapphire Substrate. *J. Phys. D: Appl. Phys.* **2017**, *50*, 395101.
- (36) Sun, H.; Wu, F.; Park, Y. J.; Al Tahtamouni, T. M.; Li, K.-H.; Alfaraj, N.; Detchprohm, T.; Dupuis, R. D.; Li, X. Influence of TMAI Preflow on AlN Epitaxy on Sapphire. *Appl. Phys. Lett.* **2017**, *110*, 192106.
- (37) Connie, A. T.; Zhao, S.; Sadaf, S. M.; Shih, I.; Mi, Z.; Du, X.; Lin, J.; Jiang, H. Optical and Electrical Properties of Mg-Doped AlN Nanowires Grown by Molecular Beam Epitaxy. *Appl. Phys. Lett.* **2015**, *106*, 213105.
- (38) Olivier, F.; Daami, A.; Licitra, C.; Templier, F. Shockley–Read–Hall and Auger Non-Radiative Recombination in GaN Based LEDs: A Size Effect Study. *Appl. Phys. Lett.* **2017**, *111*, 022104.
- (39) Zhang, L.; Chu, W.; Zheng, Q.; Benderskii, A. V.; Prezhdo, O. V.; Zhao, J. Suppression of Electron–Hole Recombination by Intrinsic Defects in 2D Monoelemental Material. *J. Phys. Chem. Lett.* **2019**, *10*, 6151–6158.
- (40) Christenson, S.; Xie, W.; Sun, Y.-Y.; Zhang, S. B. Kinetic Path towards the Passivation of Threading Dislocations in GaN by Oxygen

Impurities. *Phys. Rev. B: Condens. Matter Mater. Phys.* **2017**, *95*, 121201.

(41) Zhao, C.; Ng, T. K.; ElAfandy, R. T.; Prabaswara, A.; Consiglio, G. B.; Ajia, I. A.; Roqan, I. S.; Janjua, B.; Shen, C.; Eid, J.; Alyamani, A. Y.; El-Desouki, M. M.; Ooi, B. S. Droop-Free, Reliable, and High-Power InGaN/GaN Nanowire Light-Emitting Diodes for Monolithic Metal-Optoelectronics. *Nano Lett.* **2016**, *16*, 4616–4623.

(42) Zhao, C.; Ng, T. K.; Wei, N.; Prabaswara, A.; Alias, M. S.; Janjua, B.; Shen, C.; Ooi, B. S. Facile Formation of High-Quality InGaN/GaN Quantum-Disks-in-Nanowires on Bulk-Metal Substrates for High-Power Light-Emitters. *Nano Lett.* **2016**, *16*, 1056–1063.

(43) David, A.; Hurni, C. A.; Young, N. G.; Craven, M. D. Electrical Properties of III-Nitride LEDs: Recombination-Based Injection Model and Theoretical Limits to Electrical Efficiency and Electroluminescent Cooling. *Appl. Phys. Lett.* **2016**, *109*, 083501.

(44) Alfaraj, N.; Hussain, A. M.; Torres Sevilla, G. A.; Ghoneim, M. T.; Rojas, J. P.; Aljedaani, A. B.; Hussain, M. M. Functional Integrity of Flexible n-Channel Metal–Oxide–Semiconductor Field-Effect Transistors on a Reversibly Bistable Platform. *Appl. Phys. Lett.* **2015**, *107*, 174101.

(45) Tangi, M.; Min, J.-W.; Priante, D.; Subedi, R. C.; Anjum, D. H.; Prabaswara, A.; Alfaraj, N.; Liang, J. W.; Shakfa, M. K.; Ng, T. K.; Ooi, B. S. Observation of Piezotronic and Piezo-Phototronic Effects in n-InGaN Nanowires/Ti Grown by Molecular Beam Epitaxy. *Nano Energy* **2018**, *54*, 264–271.

(46) Ramvall, P.; Tanaka, S.; Nomura, S.; Riblet, P.; Aoyagi, Y. Observation of Confinement-Dependent Exciton Binding Energy of GaN Quantum Dots. *Appl. Phys. Lett.* **1998**, *73*, 1104–1106.

(47) Priante, D.; Tangi, M.; Min, J.-W.; Alfaraj, N.; Liang, J. W.; Sun, H.; Alhashim, H. H.; Li, X.; Albadri, A. M.; Alyamani, A. Y.; Ng, T. K.; Ooi, B. S. Enhanced Electro-Optic Performance of Surface-Treated Nanowires: Origin and Mechanism of Nanoscale Current Injection for Reliable Ultraviolet Light-Emitting Diodes. *Opt. Mater. Express* **2019**, *9*, 203–215.

(48) Scimeca, T.; Muramatsu, Y.; Oshima, M.; Oigawa, H.; Nannichi, Y. Temperature-Dependent Changes on the Sulfur-Passivated GaAs (111)A,(100), and (111)B Surfaces. *Phys. Rev. B: Condens. Matter Mater. Phys.* **1991**, *44*, 12927.

(49) Li, D.; Sumiya, M.; Fuke, S.; Yang, D.; Que, D.; Suzuki, Y.; Fukuda, Y. Selective Etching of GaN Polar Surface in Potassium Hydroxide Solution Studied by X-Ray Photoelectron Spectroscopy. *J. Appl. Phys.* **2001**, *90*, 4219–4223.

(50) Sun, J.; Rickert, K. A.; Redwing, J. M.; Ellis, A. B.; Himpsel, F. J.; Kuech, T. F. p-GaN Surface Treatments for Metal Contacts. *Appl. Phys. Lett.* **2000**, *76*, 415–417.

(51) Lee, J.-L.; Kim, J. K.; Lee, J. W.; Park, Y. J.; Kim, T. Effect of Surface Treatment by KOH Solution on Ohmic Contact Formation of p-Type GaN. *Solid-State Electron.* **1999**, *43*, 435–438.

(52) Muhammed, M. M.; Alwadai, N.; Lopatin, S.; Kuramata, A.; Roqan, I. S. High-Efficiency InGaN/GaN Quantum Well-Based Vertical Light-Emitting Diodes Fabricated on β -Ga₂O₃ Substrate. *ACS Appl. Mater. Interfaces* **2017**, *9*, 34057–34063.

(53) Ajia, I. A.; Yamashita, Y.; Lorenz, K.; Muhammed, M. M.; Spasevski, L.; Almalawi, D.; Xu, J.; Iizuka, K.; Morishima, Y.; Anjum, D. H.; Wei, N.; Martin, R. W.; Kuramata, A.; Roqan, I. S. GaN/AlGaIn Multiple Quantum Wells Grown on Transparent and Conductive (−201)-Oriented β -Ga₂O₃ Substrate for UV Vertical Light Emitting Devices. *Appl. Phys. Lett.* **2018**, *113*, 082102.

(54) Ajia, I. A.; Edwards, P. R.; Pak, Y.; Belekov, E.; Roldan, M. A.; Wei, N.; Liu, Z.; Martin, R. W.; Roqan, I. S. Generated Carrier Dynamics in V-Pit-Enhanced InGaN/GaN Light-Emitting Diode. *ACS Photonics* **2018**, *5*, 820–826.

(55) Hilgevoord, J. The Uncertainty Principle for Energy and Time. *Am. J. Phys.* **1996**, *64*, 1451.

(56) Aharonov, Y.; Reznik, B. Weighing a Closed System and the Time-Energy Uncertainty Principle. *Phys. Rev. Lett.* **2000**, *84*, 1368–1370.

(57) Pfeifer, P.; Fröhlich, J. Generalized Time-Energy Uncertainty Relations and Bounds on Lifetimes of Resonances. *Rev. Mod. Phys.* **1995**, *67*, 759.

(58) Aharonov, Y.; Massar, S.; Popescu, S. Measuring Energy, Estimating Hamiltonians, and the Time-Energy Uncertainty Relation. *Phys. Rev. A: At., Mol., Opt. Phys.* **2002**, *66*, 052107.

(59) Aharonov, Y.; Bohm, D. Time in the Quantum Theory and the Uncertainty Relation for Time and Energy. *Phys. Rev.* **1961**, *122*, 1649.

(60) Shaniv, R.; Manovitz, T.; Shapira, Y.; Akerman, N.; Ozeri, R. Toward Heisenberg-Limited Rabi Spectroscopy. *Phys. Rev. Lett.* **2018**, *120*, 243603.

(61) Randi, F.; Fausti, D.; Eckstein, M. Bypassing the Energy-Time Uncertainty in Time-Resolved Photoemission. *Phys. Rev. B: Condens. Matter Mater. Phys.* **2017**, *95*, 115132.

(62) Gabrielse, G.; Dehmelt, H. Observation of Inhibited Spontaneous Emission. *Phys. Rev. Lett.* **1985**, *55*, 67.